HHS Public Access

Author manuscript

Neuroimage. Author manuscript; available in PMC 2022 July 08.

Published in final edited form as:

Neuroimage. 2021 December 15; 245: 118688. doi:10.1016/j.neuroimage.2021.118688.

Association between brain structural network efficiency at term-equivalent age and early development of cerebral palsy in very preterm infants

Julia E. Kline[a], **Weihong Yuan**[b,c], **Karen Harpster**[d,e], **Mekibib Altaye**[f,g], **Nehal A. Parikh**[a,b,f,*]

[a]Perinatal Institute, Cincinnati Children's Hospital Medical Center, 3333 Burnet Ave, MLC 7009, Cincinnati, OH 45229, United States

[b]Pediatric Neuroimaging Research Consortium, Cincinnati Children's Hospital Medical Center, Cincinnati, OH, United States

[c]Department of Radiology, Division of Occupational Therapy and Physical Therapy, University of Cincinnati College of Medicine, Cincinnati, OH, United States

[d]Cincinnati Children's Hospital Medical Center, Cincinnati, OH, United States

[e]Department of Rehabilitation, Exercise, and Nutrition Sciences, College of Allied Health Sciences, University of Cincinnati, Cincinnati, OH, United States

[f]Department of Pediatrics, University of Cincinnati College of Medicine, Cincinnati, OH, United States

[g]Division of Biostatistics and Epidemiology, Cincinnati Children's Hospital Medical Center, Cincinnati, OH, United States

Abstract

Very preterm infants (born at less than 32 weeks gestational age) are at high risk for serious motor impairments, including cerebral palsy (CP). The brain network changes that antecede the early development of CP in infants are not well characterized, and a better understanding may suggest new strategies for risk-stratification at term, which could lead to earlier access to therapies. Graph theoretical methods applied to diffusion MRI-derived brain connectomes may help quantify the organization and information transfer capacity of the preterm brain with greater nuance than overt structural or regional microstructural changes. Our aim was to shed light on the pathophysiology of early CP development, before the occurrence of early intervention

*Corresponding author at: Perinatal Institute, Cincinnati Children's Hospital Medical Center, 3333 Burnet Ave, MLC 7009, Cincinnati, OH 45229, United States. Nehal.Parikh@cchmc.org (N.A. Parikh).

Supplementary materials

Supplementary material associated with this article can be found, in the online version, at doi:10.1016/j.neuroimage.2021.118688.

Credit authorship contribution statement

Julia E. Kline: Data curation, Formal analysis, Writing – original draft, Writing – review & editing, Investigation, Methodology, Resources, Software, Validation, Visualization. **Weihong Yuan:** Methodology, Resources, Validation, Formal analysis, Writing – review & editing. **Karen Harpster:** Data curation, Writing – review & editing, Investigation, Methodology, Resources. **Mekibib Altaye:** Methodology, Resources, Formal analysis, Validation, Writing – review & editing. **Nehal A. Parikh:** Conceptualization, Data curation, Formal analysis, Writing – review & editing, Funding acquisition, Investigation, Methodology, Project administration, Resources, Supervision.

therapies and other environmental confounders, to help identify the best early biomarkers of CP risk in VPT infants. In a cohort of 395 very preterm infants, we extracted cortical morphometrics and brain volumes from structural MRI and also applied graph theoretical methods to diffusion MRI connectomes, both acquired at term-equivalent age. Metrics from graph network analysis, especially global efficiency, strength values of the major sensorimotor tracts, and local efficiency of the motor nodes and novel non-motor regions were strongly inversely related to early CP diagnosis. These measures remained significantly associated with CP after correction for common risk factors of motor development, suggesting that metrics of brain network efficiency at term may be sensitive biomarkers for early CP detection. We demonstrate for the first time that in VPT infants, early CP diagnosis is anteceded by decreased brain network segregation in numerous nodes, including motor regions commonly-associated with CP and also novel regions that may partially explain the high rate of cognitive impairments concomitant with CP diagnosis. These advanced MRI biomarkers may help identify the highest risk infants by term-equivalent age, facilitating earlier interventions that are informed by early pathophysiological changes.

Keywords

Infant; Premature; Cerebral palsy; Magnetic resonance imaging; Diffusion MRI; White matter

1. Introduction

Across the globe, nearly 10% of babies are born preterm (Chawanpaiboon et al., 2019). Very preterm (VPT) infants are born at less than 32 weeks gestational age (GA) and disproportionally suffer from motor impairments including cerebral palsy (CP), one of the most prevalent childhood physical disabilities (Spittle et al., 2011). Approximately 8% of babies born at less than 28 weeks GA develop CP, and the percentage increases with each added week of prematurity (Smith et al., 2018). While all children with CP manifest sensorimotor impairments, up to 50% also suffer from cognitive and language impairments (Novak et al., 2012). By school age, 32–44% of VPT children exhibit signs of milder motor abnormalities than CP (Arnaud et al., 2007; Van Hus et al., 2014). Cerebral palsy is commonly diagnosed around two years of age or later. This is primarily because 30% of children who develop CP do not have any major injury on brain MRI (De Vries et al., 2011; Hubermann et al., 2016; Hadders-Algra, 2014; Benini et al., 2013). This lag in identification of the most at-risk infants causes clinicians and therapists to miss the window for intervention when neuroplasticity is maximal. Given the value of early intervention to preserve motor and cognitive ability (Spittle et al., 2015), time lost may mean increased rates of neurodevelopmental impairment in this vulnerable population. The brain network changes that antecede early development of CP in infants are not well-characterized, and a better understanding may suggest new strategies for risk-stratification at term, which could lead to earlier access to therapies.

We previously demonstrated that brain volumetrics and cortical morphometrics from term structural MRI are predictive of motor aptitude at two-years of age (Kline et al., 2020). However, more sensitive methods such as diffusion MRI are able to query the brain's microstructure in greater detail, and regional diffusion metrics (e.g., fractional anisotropy

[FA]) are more tightly linked with CP than measures of macrostructural injury (Parikh, 2016; Parikh et al., 2019; Merhar et al., 2020). On the network connectome level, graph theoretical methods applied to diffusion MRI may help quantify the organization and information transfer capacity of the preterm brain with greater nuance than overt structural or regional microstructural changes (Bullmore and Sporns, 2009; Rubinov and Sporns, 2010; Sporns and Zwi, 2004; Sporns, 2013; Bassett et al., 2017). Using graph theory, the brain's wiring diagram or connectome can be modeled as a collection of regions (nodes) and the magnitude of their interaction (edge weights). These edge weights can be anything from the total number of white matter streamlines connecting two nodes, the mean functional connectivity value between two nodes, the mean fractional anisotropy, etc. From such connectivity matrices, graph theory metrics can be calculated that quantify high-level properties of the network, which may help elucidate the biological and network underpinnings of disorders such as CP (Rubinov and Sporns, 2010; Sporns, 2013; Bassett et al., 2017).

Many graph theory metrics can be understood as measures of either functional integration or functional segregation. Functional integration is the ability of a network to rapidly combine specialized information from distant regions, while functional segregation is the ability of discrete groups of nodes to carry out specialized processing. Global efficiency (E_{glob}), or the network's inverse shortest path length, is an integration measure (Latora and Marchiori, 2001). Shorter paths do not represent physical distance, but rather represent fewer steps between regions. Local efficiency (E_{loc}) (Wang et al., 2017) is a segregation measure that is equivalent to global efficiency calculated on the neighborhood of an individual node. Clustering coefficient (CC) (Latora and Marchiori, 2001), another segregation measure, describes the fraction of a node's neighbors that are neighbors of each other, indexing the ability of nodes to cluster into sub-groups and providing a measure of network fault tolerance. Strength is the sum of all edge weights (e.g., FA) for an individual node, which makes it a surrogate measure of the microstructural integrity of all tracts traversing that region. Global efficiency, local efficiency, clustering coefficient, and strength are all altered in preterm infants and children compared to their term-born peers (Young et al., 2018; Thompson et al., 2016; Bouyssi-Kobar et al., 2019; Ballester-Plané et al., 2017; Ceschin et al., 2015), and such alterations have been correlated with illnesses of prematurity and neurodevelopmental impairment (Bouyssi-Kobar et al., 2019; Ballester-Plané et al., 2017; Ceschin et al., 2015; Gozdas et al., 2018). For instance, Young et al. (2018) reported decreased E_{glob}, E_{loc}, and CC in very preterm children compared to term-born peers at age four, and Bouyssi-Kobar and colleagues showed that bronchopulmonary dysplasia and length of oxygen support were associated with further decreased global efficiency in the preterm brain (Bouyssi-Kobar et al., 2019).

A recent international guideline recommended the combined use of structural MRI at term-equivalent age and Prechtl's General Movements Assessment (GMA) or the Hammersmith Infant Neurological Examination (HINE) at 3-4 months corrected age to facilitate early diagnosis or high-risk for CP label (Novak et al., 2017). In a large prospective cohort of VPT infants, we used this rubric to diagnose early CP and examined brain morphometry metrics from term structural MRI and graph theory metrics from term diffusion MRI as potential antecedents of abnormal motor development in a large prospective cohort of VPT infants.

Our aims were to shed light on the pathophysiology of early CP development, before the occurrence of early intervention therapies and other environmental confounders, and to help identify the best early biomarkers of CP risk in VPT infants.

2. Material and methods

2.1. Participants

We enrolled a multicenter, prospective cohort of 395 VPT infants born at or before 32 weeks GA from five level-III Greater Cincinnati area neonatal intensive care units: (1) Cincinnati Children's Hospital Medical Center, (2) University of Cincinnati Medical Center, (3) Good Samaritan Hospital, (4) Kettering Medical Center, and (5) St. Elizabeth Healthcare. Participants were recruited between September 2016 and November 2019 and were excluded if they had cyanotic heart disease or chromosomal or congenital anomalies of the central nervous system. For this study we also expected that infants with severe destructive brain injury would need to be excluded as these anatomic abnormalities do not permit accurate alignment of subject images to group atlases. The Cincinnati Children's Hospital Institutional Review Board approved this study, resulting in approval at the other sites due to reciprocity agreements. A parent or guardian of each infant gave written informed consent.

2.2. MRI data acquisition

All study infants were imaged during natural sleep between 40- and 44-weeks postmenstrual age on the same 3T Philips Ingenia scanner (Best, Netherlands) with 32 channel phase array head coil, using identical imaging parameters. A neonatal nurse and a neonatologist were present for any scans requiring positive pressure airway support. Each infant was fed 30 min prior to MRI, fitted with silicone earplugs to block scanner noise, and swaddled in a blanket and a vacuum immobilization device to promote natural sleep. We acquired MRI data as follows: diffusion MRI: echo time 88 ms, repetition time 6972 ms, flip angle 90°, field of view 160 × 160 mm^2, 80 × 79 matrix, 2 mm contiguous slices, and 5:58 min total scan time. 34 directions of diffusion gradients were applied with a b-value of 800 s/mm^2, and 4 b0 images were acquired; axial T2-weighted image: echo time 166 ms, repetition time 18,567 ms, flip angle 90°, voxel dimensions 1.0 × 1.0 × 1.0 mm^3, and 3:43 min total scan time; 3D T1-w image (magnetization-prepared rapid gradient echo): echo time 3.4 ms, repetition time 7.3 ms, flip angle 11°, voxel dimensions 1.0 × 1.0 × 1.0 mm^3, and 2:47 min total scan time; sagittal SWI: echo time 7.2 ms, repetition time 29 ms, flip angle 17°, voxel dimensions 0.57 × 0.57 × 1.0 mm^3, and 3:27 min total scan time.

2.3. Early motor examinations

At 3 to 4 months corrected age, infants returned for motor testing using the GMA and the HINE. General movements were recorded for 5 min with the calm, undressed infant placed supine (Einspieler and Prechtl, 2005; Einspieler et al., 2004). The videos were scored within 72 h by one certified examiner masked to MRI and clinical history. Any questionable videos were reviewed by a second rater from the General Movements Trust (Harpster et al., 2021). Normally developing infants should exhibit complex fidgety movements of the arms, legs, neck, and trunk. Infants with these movements received normal GMA scores and infants

lacking fidgety movements or with abnormal fidgety movements received abnormal scores. The HINE is a standard neurological examination indicated for infants between 2 and 24 months of age and comprising 26 items over 5 domains: cranial nerve function (max score of 15), posture (max score of 18), movements (max score of 6), tone (max score of 24), and reflexes and reactions (max score of 15) (Romeo et al., 2013). Each item is scored between 0 and 3, and these scores are summed to obtain an overall HINE score (range: 0–78). A HINE score below 57 is considered abnormal at this age (Romeo et al., 2013). A single trained examiner masked to clinical history and term MRI findings performed all HINE testing and GMA recording during the same visit.

2.4. Brain abnormality and CP risk scoring

A single pediatric neuroradiologist masked to clinical history assessed brain abnormality using Kidokoro's standard rubric (Kidokoro et al., 2013), which generates abnormality scores for the gray matter, white matter, deep gray matter, and cerebellum, which are subsequently summed to obtain a global brain abnormality score. Total scores of 0–3 are normal, scores of 4–7 represent mild abnormality, scores of 8–11 are moderate, and scores of 12 and higher represent severe abnormality. Using the Novak et al. early CP diagnosis guidelines (Novak et al., 2017), we labeled infants as having early CP if they had both moderate to severe injury on structural MRI (score ≥8) plus an abnormal GMA and/or an abnormal HINE score.

2.5. Structural MRI processing

We used the developing human connectome project (dHCP) pipeline (Makropoulos et al., 2018) to automatically segment the structural T2-weighted images. The dHCP performs tissue segmentation and volume estimation for each main tissue type and all cortical and subcortical structures. It also generates maturation metrics for each cortical region of the Gousias (Gousias et al., 2013; Gousias et al., 2012) neonatal atlas. As our initial structural MRI feature set, we chose four cortical maturational features that are altered by preterm birth (Kline et al., 2019): surface area, gyrification index, sulcal depth, and inner cortical curvature for the whole brain and bilaterally for all five lobes (frontal, parietal, occipital, temporal, and insular). We also examined volume of the white matter, deep gray matter, and ventricles; bilateral volume of all five lobes; bilateral volume of the main subcortical structures: the amygdala, hippocampus, caudate nucleus, lentiform nucleus, thalamus, subthalamic nucleus, and cerebellum; and unilateral volume of the corpus collosum and brainstem. To facilitate interpretability of the reported odds ratios, we divided brain volumes (originally in mm^3) by 1000 to transform them to cm^3 (mL). We also divided total and regional surface area measurements by 100 to transform them to cm^2. As sulcal depth is a unitless measure reflecting mean convexity/concavity (Makropoulos et al., 2018), we converted to a z score before calculating the associated odds ratios.

2.6. Diffusion MRI processing

We processed the b800 data using a slightly modified version of the dHCP diffusion preprocessing pipeline (Bastiani et al., 2019), correcting for susceptibility-induced distortions, eddy current artifact, and movement artifact. With Diffusion Toolkit, we generated maps of FA and performed whole-brain, deterministic fiber tracking in diffusion

space. We aligned the 122-region John's Hopkins University (JHU) (Oishi et al., 2011) neonatal brain template to create parcellated brain maps in diffusion space (Fig. 1) in a multi-step process. First, we aligned the JHU T2-weighted scan to the subject T2-weighted scan using FLIRT linear alignment in FSL (http://fsl.fmrib.ox.ac.uk/fsl/fslwiki/, version 5.0.11), and then we applied the resulting transform on the JHU parcellation file. To enhance the alignment of the fine anatomical structures, in ANTs (Avants et al., 2011), we used symmetric normalization, an elastic registration tool, to further conform the FLIRT-aligned image to subject T2-weighted space. Then we applied this second transform to the parcellation file. With a second FLIRT alignment, we registered subject T2 space to b0 space and applied this third and final transformation to the parcellation file.

2.7. Brain structural connectome construction

In MRTRIX3 (http://www.mrtrix.org, version 0.3.0), we generated symmetrical, undirected connectivity matrices, with edge weights corresponding to the mean fractional anisotropy (FA) for all streamlines connecting each pair of regions. FA is influenced by axonal density, packing, orientation, and myelination and has often been used as a surrogate measure of white matter health or maturation. We first extracted FA values for each point along each white matter streamline and then stored the paired regional means as 122 × 122 connectivity matrices. Because regional graph theory metrics are influenced by average network degree[42], we normalized by retaining the 950 strongest links for each network (the minimum number of unique nonzero connections across all connectomes was 966). This approach results in an equal average degree distribution for all networks (van Wijk et al., 2010). To ensure that our normalization was robust, we also repeated all analyses retaining the top 900 and 850 strongest links.

2.8. Graph theory metrics

We used the open-source MATLAB-compatible Brain Connectivity Toolbox (brain-connectivity-toolbox.net) to calculate our graph theory metrics. For each subject, we computed E_{glob} for the whole connectome and E_{loc}, CC, and strength for each node (n = 122).

2.9. Statistical analysis

In Stata 16.0 (StataCorp, College Station, TX), we used logistic regression to examine the association of all MRI metrics of interest with early diagnosis of CP, coded as 0 (early CP) or 1 (no CP). We coded early CP diagnosis as 0 rather than 1 to facilitate clinical interpretation of our results, because we expected our advanced MRI biomarkers would exhibit a negative association with cerebral palsy (i.e., the higher the graph theory or morphometric measure, the lower the risk of CP). We corrected for (1) just postmenstrual age (PMA) at scan and (2) PMA at scan, gestational age (GA), sex, bronchopulmonary dysplasia (BPD), retinopathy of prematurity (ROP), and maternal magnesium therapy. We selected these variables because previous work associated them with motor outcome in VPT infants. BPD is a chronic lung disease affecting preterm infants who often require mechanical ventilation or continuous positive airway pressure and supplementary oxygen (Davidson and Berkelhamer, 2017). It is related to later neurodevelopmental deficits including cerebral palsy (Van Marter et al., 2011) and poorer cognitive (Singer et al.,

2001) and language outcomes (Short et al., 2003; Natarajan et al., 2012). ROP, a severe eye disease, is also linked to excessive use of oxygen in the neonatal period (Morken et al., 2019). Severe ROP is associated with delayed white matter maturation, poorer cognitive and motor scores (Glass et al., 2017), and lower IQ in late childhood (Molloy et al., 2016). BPD and ROP tend to co-occur, but they are independently predictive of neurodevelopmental impairment (Schmidt et al., 2003). For all regional volume and surface area metrics, we also included either total tissue volume or total cortical surface area, respectively, as regression covariates to control for the effect of differing brain sizes. We applied Benjamini Hochberg false discovery rate (FDR) correction to account for all 367 graph theory metrics (1 global measure + 3 regional measures x 122 nodes) and all 72 structural MRI metrics tested. Because E_{glob}, E_{loc}, and CC, are small numbers theoretically ranging from 0 to 1, we transformed the values of all graph theory metrics to z scores before calculating the associated odds ratios.

To identify possible exclusion bias, we compared the baseline characteristics of the final cohort to those of the excluded infants. We used Fischer's exact test for binary variables and either a Student's *t*-test or a Mann-Whitney U test for continuous variables, after assessing normality with a Shapiro Wilks test. For this bias analysis, a *p*-value of <0.05 indicated significance.

2.10. Data and code availability statement

Code used in this analysis and derived data that support the conclusions of this study are available upon direct request to the corresponding author.

3. Results

Of our initial 395 participants, 364 had either structural or diffusion data at term and early CP outcome. A statistical comparison of the baseline variables for these 364 infants versus the 31 excluded infants can be found in Table 1. Excluded infants were statistically more likely to have BPD and, as expected, severe brain injury than included infants. Subdividing by MRI modality, 326 infants had high-quality artifact-free T2-w images that were successfully processed by the dHCP pipeline. 312 returned for follow-up motor assessments, and 32 (10.3%) of these infants were diagnosed with early CP. 327 infants had high-quality diffusion MRI with optimal template alignment, 313 returned, and of these 34 (10.9%) were diagnosed with early CP. All analyses were carried out on final cohorts of 312 and 313 for structural and diffusion MRI, respectively.

When correcting for PMA only, total tissue volume (OR [95% CI]: 1.03 [1.02, 1.04], $p = 6.11 \times 10^{-8}$), total surface area (1.01 [1.01, 1.02], $p = 1.74 \times 10^{-6}$), and total sulcal depth (2.32 [1.43, 3.70], $p = 6.96 \times 10^{-4}$) of the very preterm brain were all negatively correlated with early CP diagnosis. Regionally, bilateral volume of the thalamus (right: 16.67 [3.7, 100.00], $p = 2.53 \times 10^{-4}$; left: 11.11 [2.70, 50.00], $p = 9.52 \times 10^{-4}$), total volume of the deep gray matter (including the thalamus and also the caudate, lentiform, and subthalamic nuclei: 1.85 [1.32, 2.56], $p = 3.90 \times 10^{-4}$), and volume of the brainstem (6.67 [0.05, 0.47], $p = 1.10 \times 10^{-3}$) were all negatively associated with CP, whereas ventricular volume (0.83 [0.76, 0.92], $p = 1.43 \times 10^{-4}$) was positively associated. There were no significant

associations with any curvature or gyrification metrics. When correcting for all covariates of interest, total tissue volume (1.02 [1.01,1.03], $p = 1.42 \times 10^{-4}$), total surface area (1.01 [1.003, 1.01], $p = 8.11 \times 10^{-4}$), bilateral thalamic volume (right: 12.5 [2.70, 50.00], $p = 1.26 \times 10^{-3}$; left: 9.09 [2.13, 50.00], $p = 3.11 \times 10^{-3}$), and volume of the deep gray matter (1.72 [1.22, 2.50], $p = 2.34 \times 10^{-3}$) remained negatively associated with CP, and ventricular volume (0.85 [0.76, 0.94], $p = 2.03 \times 10^{-3}$) remained positively associated (Fig. 2).

Graph theory metrics of network efficiency were associated with early CP in numerous brain regions. Correcting for PMA only, global efficiency of the entire brain network was negatively associated with early CP diagnosis (OR [95% CI]: 3.70 [2.27, 5.88], $p = 6.39 \times 10^{-8}$). The same was true for local efficiency in 72 regions, clustering coefficient in 28 regions, and strength in 24 regions (See Supplementary Table 1 for all significant regions and their p-values when correcting for PMA only). When correcting for all covariates of interest, global efficiency remained negatively associated with early CP (3.13 [1.85, 5.26], 1.76×10^{-5}). Local efficiency, clustering coefficient, and strength remained negatively associated with early CP in 41, 9, and 10 nodes, respectively (Table 2; Figs. 3–5). Segregation metrics (E_{loc} and CC) were decreased with CP diagnosis in multiple sensorimotor regions previously reported in diffusion MRI studies to be associated with established CP (e.g., the subcortical nuclei, the precentral and postcentral gyrus, and the cerebellum) and in a few novel ROIs in the frontal, parietal, and occipital lobes. Strength values that were significantly related to early CP diagnosis occurred primarily in major white matter tracts including the stria terminalis, the left corpus callosum, left posterior corona radiata, left pontine crossing tract, right tapetum, right corticospinal tract, left posterior thalamic radiations, and right fornix. When testing the same networks with the top 900 and 850 strongest connections retained, E_{glob} remained highly significant ($p = 2.31 \times 10^{-5}$ for 900 and $p = 3.07 \times 10^{-5}$ for 850 links). See Supplementary Table 1 for all significant regional metrics at different network density levels.

4. Discussion

In our cohort of VPT infants, early development of CP was anteceded by decreased global brain efficiency by term-equivalent age and decreased graph theory measures of functional segregation in sensorimotor regions known to be impacted in CP and also in novel regions. A decrease in regional GT metrics in multiple nodes or a decrease in whole brain global efficiency were associated with significantly elevated odds of early CP diagnosis. For the morphometry measures, a decrease in total surface area, whole-brain sulcal depth, total volume, or multiple regional brain volumes was associated with significantly elevated odds of early CP diagnosis. These findings, and the more widespread regional significance of the graph metrics, suggests that altered brain network efficiency may be more sensitive to the early brain changes associated with CP than morphometric abnormalities. Our analysis also suggests that the early development of CP is characterized by widespread brain network alteration rather than damage to isolated regions or tracts, for instance to the motor nuclei and motor cortex alone. Using a data-driven approach, our study is also the first to identify numerous nodes and pathways that are involved in the etiology of CP after preterm birth.

After correcting for known risk factors of CP, decreased global efficiency of the preterm structural connectome was associated with early CP diagnosis, independent of potential confounders. Local efficiency of the preterm brain was inversely associated with CP in the highest number of nodes of any metric tested ($n = 41$), most strongly in the left and right thalamus, right corpus callosum, right fornix, and right cingulate gyrus. Strength values tied to early CP risk mainly occurred in the major motor tracts including the left posterior corona radiata (carrying information from the precentral gyrus of the motor cortex Song, 2007), left pontine crossing tract (a pathway involved in the planning and control of precise dexterous movements Haines and Mihailoff, 2017), right corticospinal tract (relaying information from the sensory cortex and the major spinal pathways that control voluntary movements Van Wittenberghe and Peterson, 2020), and the left posterior thalamic radiations (connecting the thalamus to the occipital cortex). The overall picture emergent from graph theory suggests that CP is associated with decreased integrity of the major motor tracts, as indexed by strength. Compromised integrity of these pathways would reduce overall information processing capability (as indexed by E_{glob}) and local modular processing (as indexed by E_{loc} and CC), and we indeed see a concurrent downregulation in these metrics with early CP, especially in the precentral and postcentral gyrus, subcortical nuclei, cerebellum, and accessory regions in the parietal and occipital cortex that facilitate higher-order spatial processing. Both segregation metrics were significantly decreased with early CP in the right corpus callosum, right cingulate gyrus, left and right thalamus, right inferior cerebral peduncle, left and right cerebellar hemisphere, and right middle occipital gyrus, which suggests that these areas may be the main loci of compromised local information processing.

Our study corroborates other literature regarding which brain regions are most impacted by CP. In a systematic review of diffusion MRI studies of older children with established CP, the most common finding across 22 studies was reduced FA of the CST, indicating compromised integrity of this tract (reported by 17 studies) (Scheck et al., 2012). The posterior thalamic radiations, corticobulbar tract, corpus callosum, posterior limb of the internal capsule, and superior thalamic radiations were also implicated in the pathophysiology of CP by at least 3 papers each (Scheck et al., 2012), with reduced FA of these tracts in CP populations being the predominant findings. These findings highlight the importance of sensory as well as motor white matter tracts in the development of CP, with a handful of outcome studies reporting that integrity of the sensorimotor thalamic pathways exert more influence on sensory and motor function than the descending corticomotor pathways. For instance, Rose et al. illustrated that streamline count for the sensorimotor thalamic projections was more highly correlated with paretic hand function in CP than the same metric from the corticospinal tracts (Rose et al., 2011). Hoon and colleagues likewise demonstrated that PTR injury was correlated with impaired contralateral touch threshold, proprioception, and with motor impairment severity (Hoon et al., 2009). Pannek et al. (2014) performed a diffusion MRI-based structural connectivity analysis and probabilistic tractography in 50 children with unilateral CP. They identified reduced integrity in motor pathways such as the CST and the thalamocortical projections and in novel association pathways, including between the postcentral gyrus and superior frontal lobe, precentral gyrus and insular cortex, and superior frontal lobe and superior parietal lobe. In children with bilateral CP and periventricular leukomalacia, voxel-based analysis

demonstrated reduced FA in commonly-reported motor tracts and also in optic tracts, including the posterior thalamic radiations, and in the fornix and cingulum (Arrigoni et al., 2016). These combined results triangulate that white matter damage in CP is widespread across the whole brain and not restricted to sensorimotor connections. Our study suggests that such widespread changes can be observed at an early age before confounding by early intervention therapies and developmental neuroplasticity.

Our study also suggests unique regional vulnerabilities anteceding CP development in the VPT brain, especially those related to visuospatial processing and higher-order cognitive functions. We identified decreased segregation measures in a number of novel regions including the left angular gyrus, which is involved in memory, attention, and spatial cognition (Seghier, 2013), and the left and right lateral fronto-orbital gyri, which contain the inferior frontal gyrus, a major hub of language comprehension and production (Ishkhanyan et al., 2020). Associations were also seen in the right fusiform gyrus, which is involved with higher-order visual processing and is implicated in childhood visual-motor deficits (Sripada et al., 2015), and the right middle occipital gyrus, which engages in spatial processing of auditory and tactile stimuli (Renier et al., 2010). Segregation metrics in the high risk group were also diminished in brain regions commonly associated with memory and cognition, such as the left superior frontal gyrus, which contributes to working memory (du Boisgueheneuc et al., 2006), the cingulate gyrus, which plays a role in learning, memory, and emotion, the middle occipital gyrus, which is involved in object recognition (Pennick and Kana, 2012), and also in the amygdala and hippocampus and their major output pathways, i.e. the stria terminalis and the fornix. These findings are novel but unsurprising, given that CP is frequently associated with non-motor symptoms such as disrupted sensation, perception, behavior, learning, and communication. As higher cognitive functions are affected in up to 50% of children with CP, the novel associations with graph theory segregation metrics in these regions suggest that they are early antecedents of these abnormalities.

Several studies utilizing different diffusion MRI modeling techniques have identified varying degrees of white matter/brain network involvement with later motor outcomes. In a small tract-based spatial statistics study of 12 infants with perinatal brain injury, reduced FA was seen in nearly all white matter tracts in the CP group (Merhar et al., 2020). In contrast, in a cohort of VPT infants, fixel-based metrics from the Constrained Spherical Deconvolution model were only associated with two-year Bayley-III motor scores in the splenium of the corpus callosum, right corticospinal tracts, and midbrain (all motor areas). When gestational age was added as a covariate, only an association in the right CST remained. Yang et al. reported reduced strength, clustering coefficient, and local efficiency in VPT children at four years of age, notably in the lateral frontal regions, middle and superior temporal regions, cingulate, precuneus, and lateral occipital regions (Young et al., 2018). However, they did not identify an association with visuomotor ability, possibly due to their small sample size. We believe that our large sample size and meticulous template alignment, i.e., multi-step linear and non-linear alignment with visual inspection of the deep structures, allowed us to identify robust associations between early CP and graph theory metrics in multiple brain regions.

In our study, a few morphometric antecedents were significantly associated with early CP risk after full covariate correction, including bilateral thalamic volume, volume of the deep gray matter, volume of the brainstem, volume of the ventricles, total tissue volume, and total surface area. Several previous studies have reported correlations between brain tissue volumes at term-equivalent age and later motor ability/impairment (Setänen et al., 2016; Bolk et al., 2018; Gui et al., 2019; Keunen et al., 2016; Spittle et al., 2010; Limperopoulos et al., 2014) (see Keunen et al., 2012 for a systematic review). We previously identified a strong association of thalamic volume and cortical surface area with two year motor ability in a smaller VPT cohort (Kline et al., 2020). However, the associations we identified between early CP and graph theory metrics involved many more regions than those showing overt morphometric alterations. Past studies that tested diffusion MRI metrics were more likely to report identification of one or more significant prognostic biomarkers compared to volumetric MRI studies (Parikh, 2016), which agrees with our current analysis. Our study suggests that a more complete picture of the vulnerabilities present in early CP can be gleaned by analyzing the higher-order network properties of the brain, rather than focusing on the morphology of any specific region. These findings are also consistent with the fact that destructive macroscopic brain injuries such as cystic periventricular leukomalacia are far less prevalent now compared to 20 years ago (Hamrick et al., 2004).

Our large sample size was a major strength of the study. Additionally, we corrected for covariates that are pertinent to motor development to identify independent early antecedents of CP. We were limited by the lack of a clinical CP diagnosis at two years of age in this population. However, we used the most predictive set of early diagnostic tools currently available for CP detection before five months of age. Our study also had a selection bias in that the excluded participants (those for whom the data processing pipelines or template alignment failed) were more likely to have BPD and severe brain injury than the included participants. However, the fact that we identified such a strong association of graph theory metrics with early CP risk while correcting for multiple confounders is promising, as better early developmental biomarkers are specifically needed in infants who lack structural brain abnormalities on term MRI. Using these graph biomarkers in combination with other novel biomarkers to predict early CP remains an end goal of our work.

5. Conclusion

We demonstrate for the first time that in VPT infants, early CP diagnosis is anteceded by decreased brain network segregation in numerous nodes, including motor regions commonly-associated with CP (the thalamus, cerebellum, and the major sensorimotor white matter tracts) and also in novel regions such as the middle occipital gyrus and the superior frontal gyrus, which may partially explain the high rate of cognitive impairments concomitant with CP diagnosis. These advanced MRI biomarkers may detect more of the brain alterations accompanying early CP than overt brain abnormalities. These findings cannot as of yet be applied to patient care. More research would be needed to define population metric norms, and novel, efficient software would be required for brain network analysis in a clinical setting. Follow up studies are needed to verify that graph metrics correlate with CP diagnosis at age two and with cognitive impairments in this vulnerable population. We are currently conducting these additional analyses in our longitudinal cohort.

Supplementary Material

Refer to Web version on PubMed Central for supplementary material.

Acknowledgments

This research was supported by grants R01-NS094200-05 and R01-NS096037-03 from the National Institute of Neurological Disorders and Stroke (NINDS), R01-EB029944-01 from National Institute of Biomedical Imaging and Bioengineering (NIBIB), and R21-HD094085 from the Eunice Shriver Kennedy National Institute of Child Health and Human Development (NICHD). We sincerely thank the parents of infants that participated in our study and the Cincinnati Infant Neurodevelopment Early Prediction Study (CINEPS) Investigators: Principal Investigator: Nehal A. Parikh, DO, MS. Collaborators (in alphabetical order): Mekibib Altaye, PhD, Anita Arnsperger, RRT, Traci Beiersdorfer, RN BSN, Kaley Bridgewater, RT(MR) CNMT, Tanya Cahill, MD, Kim Cecil, PhD, Kent Dietrich, RT, Christen Distler, BSN RNC-NIC, Juanita Dudley, RN BSN, Brianne Georg, BS, Cathy Grisby, RN BSN CCRC, Lacey Haas, RT(MR) CNMT, Karen Harpster, PhD, OT/RL, Lili He, PhD, Scott K. Holland, PhD, V.S. Priyanka Illapani, MS, Kristin Kirker, CRC, Julia E. Kline, PhD, Beth M. Kline-Fath, MD, Hailong Li, PhD, Matt Lanier, RT(MR) RT(R), Stephanie L. Merhar, MD MS, Greg Muthig, BS, Brenda B. Poindexter, MD MS, David Russell, JD, Kari Tepe, BSN RNC-NIC, Leanne Tamm, PhD, Julia Thompson, RN BSN, Jean A. Tkach, PhD, Hui Wang, PhD, Jinghua Wang, PhD, Brynne Williams, RT(MR) CNMT, Kelsey Wineland, RT(MR) CNMT, Sandra Wuertz, RN BSN CCRP, Donna Wuest, AS, Weihong Yuan, PhD.

Biomarkers Abbreviations:

very preterm
VPT

gestational age
GA

cerebral palsy
CP

General Movements Assessment
GMA

Hammersmith Infant Neurological Examination
HINE

developing human connectome project
dHCP

bronchopulmonary dysplasia
BPD

fractional anisotropy
FA

retinopathy of prematurity
ROP

global efficiency
Eg_{lob}

local efficiency

E_{loc}

clustering coefficient

CC

References

Chawanpaiboon S, et al. , 2019. Global, regional, and national estimates of levels of preterm birth in 2014: a systematic review and modelling analysis. Lancet Glob. Health 7 (1), e37–e46. [PubMed: 30389451]

Spittle AJ, et al. , 2011. Neonatal white matter abnormality predicts childhood motor impairment in very preterm children. Dev. Med. Child Neurol doi:10.1111/j.1469-8749.2011.04095.x.

Smith DD, Sagaram D, Miller R, Gyamfi-Bannerman C, 2018. Risk of cerebral palsy by gestational age among pregnancies at-risk for preterm birth. J. Matern. Neonatal Med 0, 1–5.

Novak I, Hines M, Goldsmith S, Barclay R, 2012. Clinical prognostic messages from a systematic review on cerebral palsy. Pediatrics 130 (5). doi:10.1542/peds.2012-0924.

Arnaud C, et al. , 2007. Prevalence and associated factors of minor neuromotor dysfunctions at age 5 years in prematurely born children: the EPIPAGE study. Arch. Pediatr. Adolesc. Med 161, 1053–1061. [PubMed: 17984407]

Van Hus JW, Potharst ES, Jeukens-Visser M, Kok JH, Van Wassenaer-Leemhuis AG, 2014. Motor impairment in very preterm-born children: links with other developmental deficits at 5 years of age. Dev. Med. Child Neurol 56, 587–594. [PubMed: 24926490]

De Vries LS, van Haastert IC, Benders MJNL, Groenendaal F, 2011. Myth: cerebral palsy cannot be predicted by neonatal brain imaging. Semin. Fetal Neonatal Med doi:10.1016/j.siny.2011.04.004.

Hubermann L, Boychuck Z, Shevell M, Majnemer A, 2016. Age at referral of children for initial diagnosis of cerebral palsy and rehabilitation. J. Child Neurol doi:10.1177/0883073815596610.

Hadders-Algra M, 2014. Early diagnosis and early intervention in cerebral palsy. Front. Neurol doi:10.3389/fneur.2014.00185.

Benini R, Dagenais L, Shevell MI, 2013. Normal imaging in patients with cerebral palsy: what does it tell us? J. Pediatr doi:10.1016/j.jpeds.2012.07.044.

Spittle A, Orton J, Anderson PJ, Boyd R, Doyle LW, 2015. Early developmental intervention programmes provided post hospital discharge to prevent motor and cognitive impairment in preterm infants. Cochrane Database Syst. Rev 11, CD005495.

Kline JE, Sita Priyanka Illapani V, He L, Parikh NA, 2020. Automated brain morphometric biomarkers from MRI at term predict motor development in very preterm infants. NeuroImage Clin. doi:10.1016/j.nicl.2020.102475.

Parikh NA, 2016. Advanced neuroimaging and its role in predicting neurodevelopmental outcomes in very preterm infants. Semin. Perinatol 40, 530–541. [PubMed: 27863706]

Parikh NA, Hershey A, Altaye M, 2019. Early detection of cerebral palsy using sensorimotor tract biomarkers in very preterm infants. Pediatr. Neurol doi:10.1016/j.pediatrneurol.2019.05.001.

Merhar SL, et al. , 2020. Neonatal functional and structural connectivity are associated with cerebral palsy at two years of age. Am. J. Perinatol 37, 137–145. [PubMed: 30919395]

Bullmore E, Sporns O, 2009. Complex brain networks: graph theoretical analysis of structural and functional systems. Nat. Rev. Neurosci 10, 186–198. [PubMed: 19190637]

Rubinov M, Sporns O, 2010. Complex network measures of brain connectivity: uses and interpretations. Neuroimage 52, 1059–1069. [PubMed: 19819337]

Sporns O, Zwi JD, 2004. The small world of the cerebral cortex. Neuroinformatics 2, 145–162. [PubMed: 15319512]

Sporns O, 2013. Structure and function of complex brain networks. Dialogues Clin. Neurosci 15, 247–262. [PubMed: 24174898]

Bassett DS, Khambhati AN, Grafton ST, 2017. Emerging frontiers of neuroengineering: a network science of brain connectivity. Annu. Rev. Biomed. Eng 19, 327–352. [PubMed: 28375650]

Latora V, Marchiori M, 2001. Efficient behavior of small-world networks. Phys. Rev. Lett 87, 198701. [PubMed: 11690461]

Wang Y, Ghumare E, Vandenberghe R, Dupont P, 2017. Comparison of different generalizations of clustering coefficient and local efficiency for weighted undirected graphs. Neural Comput. doi:10.1162/NECO_a_00914.

Young JM, et al. , 2018. Altered white matter development in children born very preterm. Brain Struct. Funct 223, 2129–2141. [PubMed: 29380120]

Thompson DK, et al. , 2016. Structural connectivity relates to perinatal factors and functional impairment at 7 years in children born very preterm. Neuroimage 134, 328–337. doi:10.1016/j.neuroimage.2016.03.070. [PubMed: 27046108]

Bouyssi-Kobar M, De Asis-Cruz J, Murnick J, Chang T, Limperopoulos C, 2019. Altered functional brain network integration, segregation, and modularity in infants born very preterm at term-equivalent age. J. Pediatr 213, 13–21 e1. [PubMed: 31358292]

Ballester-Plané J, et al. , 2017. Whole-brain structural connectivity in dyskinetic cerebral palsy and its association with motor and cognitive function. Hum. Brain Mapp 38, 4594–4612. [PubMed: 28608616]

Ceschin R, Lee VK, Schmithorst V, Panigrahy A, 2015. Regional vulnerability of longitudinal cortical association connectivity: associated with structural network topology alterations in preterm children with cerebral palsy. NeuroImage. Clin 9, 322–337. [PubMed: 26509119]

Gozdas E, et al. , 2018. Altered functional network connectivity in preterm infants: antecedents of cognitive and motor impairments? Brain Struct. Funct 223, 3665–3680. [PubMed: 29992470]

Novak I, et al. , 2017. Early, accurate diagnosis and early intervention in cerebral palsy: advances in diagnosis and treatment. JAMA Pediatr. doi:10.1001/jamapediatrics.2017.1689.

Einspieler C, Prechtl HFR, 2005. Prechtl's assessment of general movements: a diagnostic tool for the functional assessment of the young nervous system. Ment. Retard. Dev. Disabil. Res. Rev doi:10.1002/mrdd.20051.

Einspieler C, Prechtl H, Bos A, Ferrari F, Cioni G, 2004. Prechtl's Method on the Qualitative Assessment of General Movements in preterm, Term and Young Infants. London Mac Keith Press.

Harpster K, et al. , 2021. Associations between early structural mri, hammersmith infant neurological exam, and general movements assessment in very preterm infants. J. Pediatr doi:10.1016/j.jpeds.2020.12.056.

Romeo DMM, Cioni M, Palermo F, Cilauro S, Romeo MG, 2013. Neurological assessment in infants discharged from a neonatal intensive care unit. Eur. J. Paediatr. Neurol doi:10.1016/j.ejpn.2012.09.006.

Kidokoro H, Neil JJ, Inder TE, 2013. New MR imaging assessment tool to define brain abnormalities in very preterm infants at term. Am. J. Neuroradiol 34, 2208–2214. [PubMed: 23620070]

Makropoulos A, et al. , 2018. The developing human connectome project: a minimal processing pipeline for neonatal cortical surface reconstruction. Neuroimage 173, 88–112. [PubMed: 29409960]

Gousias IS, et al. , 2013. Magnetic resonance imaging of the newborn brain: automatic segmentation of brain images into 50 anatomical regions. PLoS ONE doi:10.1371/journal.pone.0059990.

Gousias IS, et al. , 2012. Magnetic resonance imaging of the newborn brain: manual segmentation of labelled atlases in term-born and preterm infants. Neuroimage doi:10.1016/j.neuroimage.2012.05.083.

Kline JE, Illapani VSP, He L, Altaye M, Parikh NA, 2019. Retinopathy of prematurity and bronchopulmonary dysplasia are independent antecedents of cortical maturational abnormalities in very preterm infants. Sci. Rep 9, 1–10. [PubMed: 30626917]

Bastiani M, et al. , 2019. Automated processing pipeline for neonatal diffusion MRI in the developing human connectome project. Neuroimage doi:10.1016/j.neuroimage.2018.05.064.

Oishi K, et al. , 2011. Multi-contrast human neonatal brain atlas: application to normal neonate development analysis. Neuroimage doi:10.1016/j.neuroimage.2011.01.051.

Avants BB, et al. , 2011. A reproducible evaluation of ANTs similarity metric performance in brain image registration. Neuroimage doi:10.1016/j.neuroimage.2010.09.025.

van Wijk BCM, Stam CJ, Daffertshofer A, 2010. Comparing brain networks of different size and connectivity density using graph theory. PLoS ONE doi:10.1371/journal.pone.0013701.

Davidson L, Berkelhamer S, 2017. Bronchopulmonary dysplasia: chronic lung disease of infancy and long-term pulmonary outcomes. J. Clin. Med doi:10.3390/jcm6010004.

Van Marter LJ, et al. , 2011. Does bronchopulmonary dysplasia contribute to the occurrence of cerebral palsy among infants born before 28 weeks of gestation? Arch. Dis. Child. Fetal Neonatal Ed. doi:10.1136/adc.2010.183012.

Singer LT, et al. , 2001. Preschool language outcomes of children with history of bronchopulmonary dysplasia and very low birth weight. J. Dev. Behav. Pediatr doi:10.1097/00004703-200102000-00003.

Short EJ, et al. , 2003. Cognitive and academic consequences of bronchopulmonary dysplasia and very low birth weight: 8-year-old outcomes. Pediatrics doi:10.1542/peds.112.5.e359.

Natarajan G, et al. , 2012. Outcomes of extremely low birth weight infants with bronchopulmonary dysplasia: impact of the physiologic definition. Early Hum. Dev doi:10.1016/j.earlhumdev.2011.12.013.

Morken TS, Dammann O, Skranes J, Austeng D, 2019. Retinopathy of prematurity, visual and neurodevelopmental outcome, and imaging of the central nervous system. Semin. Perinatol doi:10.1053/j.semperi.2019.05.012.

Glass TJA, et al. , 2017. Severe retinopathy of prematurity predicts delayed white matter maturation and poorer neurodevelopment. Arch. Dis. Child. Fetal Neonatal Ed doi:10.1136/archdischild-2016-312533.

Molloy CS, Anderson PJ, Anderson VA, Doyle LW, 2016. The long-term outcome of extremely preterm (<28 weeks' gestational age) infants with and without severe retinopathy of prematurity. J. Neuropsychol 10, 276–294. [PubMed: 25809467]

Schmidt B, et al. , 2003. Impact of bronchopulmonary dysplasia, brain injury, and severe retinopathy on the outcome of extremely low-birth-weight infants at 18 months. JAMA 289 (9), 1124–1129. doi:10.1001/jama.289.9.1124. [PubMed: 12622582]

Song YM, 2007. Somatotopic organization of motor fibers in the corona radiata in monoparetic patients with small subcortical infarct. Stroke doi:10.1161/STROKEAHA.106.480632.

Haines DE, Mihailoff GA, 2017. Fundamental Neuroscience for Basic and Clinical Applications, 5th ed. Fundamental Neuroscience for Basic and Clinical Applications: Fifth Edition.

Van Wittenberghe IC, Peterson DC, 2020. Neuroanatomy, Corticospinal Tract Lesion. StatPearls.

Scheck SM, Boyd RN, Rose SE, 2012. New insights into the pathology of white matter tracts in cerebral palsy from diffusion magnetic resonance imaging: a systematic review. Dev. Med. Child Neurol 54, 684–696. [PubMed: 22646844]

Rose S, Guzzetta A, Pannek K, Boyd R, 2011. MRI structural connectivity, disruption of primary sensorimotor pathways, and hand function in cerebral palsy. Brain Connect. 1, 309–316. [PubMed: 22432420]

Hoon AHJ, et al. , 2009. Sensory and motor deficits in children with cerebral palsy born preterm correlate with diffusion tensor imaging abnormalities in thalamocortical pathways. Dev. Med. Child Neurol 51, 697–704. [PubMed: 19416315]

Pannek K, Boyd RN, Fiori S, Guzzetta A, Rose SE, 2014. Assessment of the structural brain network reveals altered connectivity in children with unilateral cerebral palsy due to periventricular white matter lesions. NeuroImage Clin. 5, 84–92. [PubMed: 25003031]

Arrigoni F, et al. , 2016. Whole-brain DTI assessment of white matter damage in children with bilateral cerebral palsy: evidence of involvement beyond the primary target of the anoxic insult. Am. J. Neuroradiol 37, 1347 LP –1353. [PubMed: 26988814]

Seghier ML, 2013. The angular gyrus: multiple functions and multiple subdivisions. Neuroscientist 19, 43–61 a Rev. J. bringing Neurobiol. Neurol. Psychiatry. [PubMed: 22547530]

Ishkhanyan B, et al. , 2020. Anterior and posterior left inferior frontal gyrus contribute to the implementation of grammatical determiners during language production. Front. Psychol 11, 685. [PubMed: 32395113]

Sripada K, et al. , 2015. Visual-motor deficits relate to altered gray and white matter in young adults born preterm with very low birth weight. Neuroimage doi:10.1016/j.neuroimage.2015.01.019.

Renier LA, et al. , 2010. Preserved functional specialization for spatial processing in the middle occipital gyrus of the early blind. Neuron 68, 138–148. [PubMed: 20920797]

du Boisgueheneuc F, et al. , 2006. Functions of the left superior frontal gyrus in humans: a lesion study. Brain 129, 3315–3328. [PubMed: 16984899]

Pennick MR, Kana RK, 2012. Specialization and integration of brain responses to object recognition and location detection. Brain Behav. 2, 6–14. [PubMed: 22574269]

Setänen S, et al. , 2016. The motor profile of preterm infants at 11y of age. Pediatr. Res doi:10.1038/pr.2016.90.

Bolk J, et al. , 2018. Visual-motor integration and fine motor skills at 6 years of age and associations with neonatal brain volumes in children born extremely preterm in Sweden: a population-based cohort study. BMJ Open doi:10.1136/bmjopen-2017-020478.

Gui L, et al. , 2019. Longitudinal study of neonatal brain tissue volumes in preterm infants and their ability to predict neurodevelopmental outcome. Neuroimage 185, 728–741. [PubMed: 29908311]

Keunen K, et al. , 2016. Brain volumes at term-equivalent age in preterm infants: imaging biomarkers for neurodevelopmental outcome through early school age. J. Pediatr doi:10.1016/j.jpeds.2015.12.023.

Spittle AJ, et al. , 2010. Reduced cerebellar diameter in very preterm infants with abnormal general movements. Early Hum. Dev doi:10.1016/j.earlhumdev.2009.11.002.

Limperopoulos C, et al. , 2014. Injury to the premature cerebellum: outcome is related to remote cortical development. Cereb. Cortex doi:10.1093/cercor/bhs354.

Keunen K, et al. , 2012. Brain tissue volumes in preterm infants: prematurity, perinatal risk factors and neurodevelopmental outcome: a systematic review. J. Matern. Neonatal Med. 25, 89–100 Off. J. Eur. Assoc. Perinat. Med. Fed. Asia Ocean. Perinat. Soc. Int. Soc. Perinat. Obstet. Suppl 1.

Hamrick SEG, et al. , 2004. Trends in severe brain injury and neurodevelopmental outcome in premature newborn infants: the role of cystic periventricular leukomalacia. J. Pediatr 145, 593–599. [PubMed: 15520756]

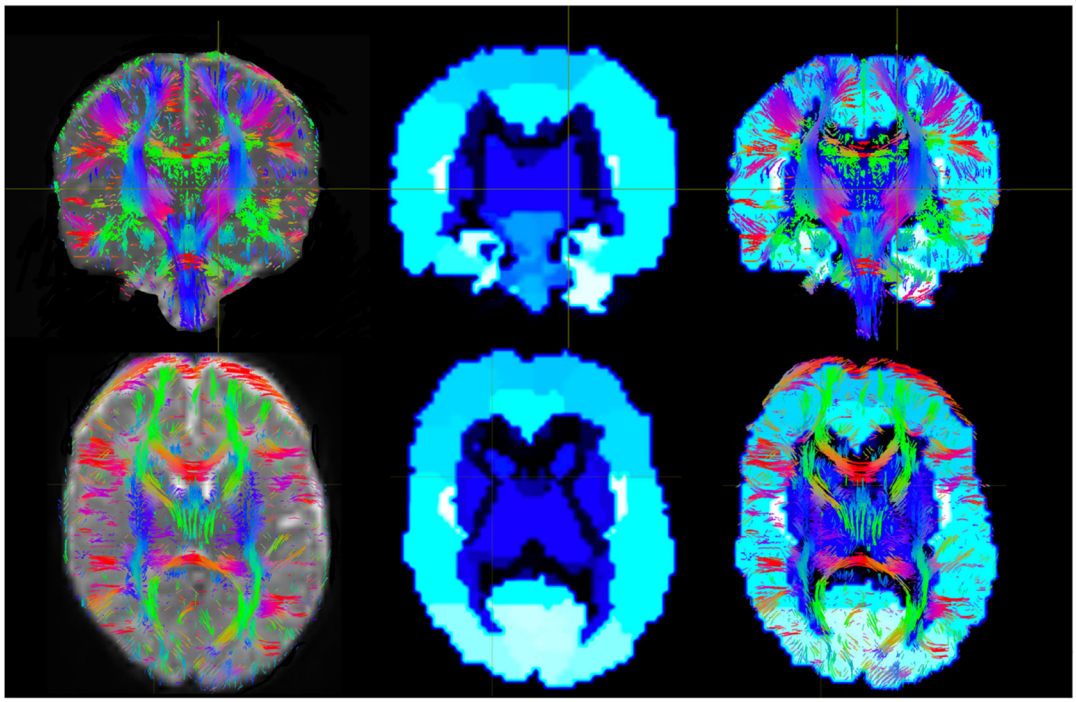

Fig. 1.

Alignment (3rd column) of the 122-region JHU atlas (2nd column) with diffusion space tractography (1st column) for a female very preterm infant, born at a gestational age of 31.86 weeks. From here, we calculated the mean fractional anisotropy for all streamlines connecting each regional pair as a 122 × 122 symmetrical matrix.

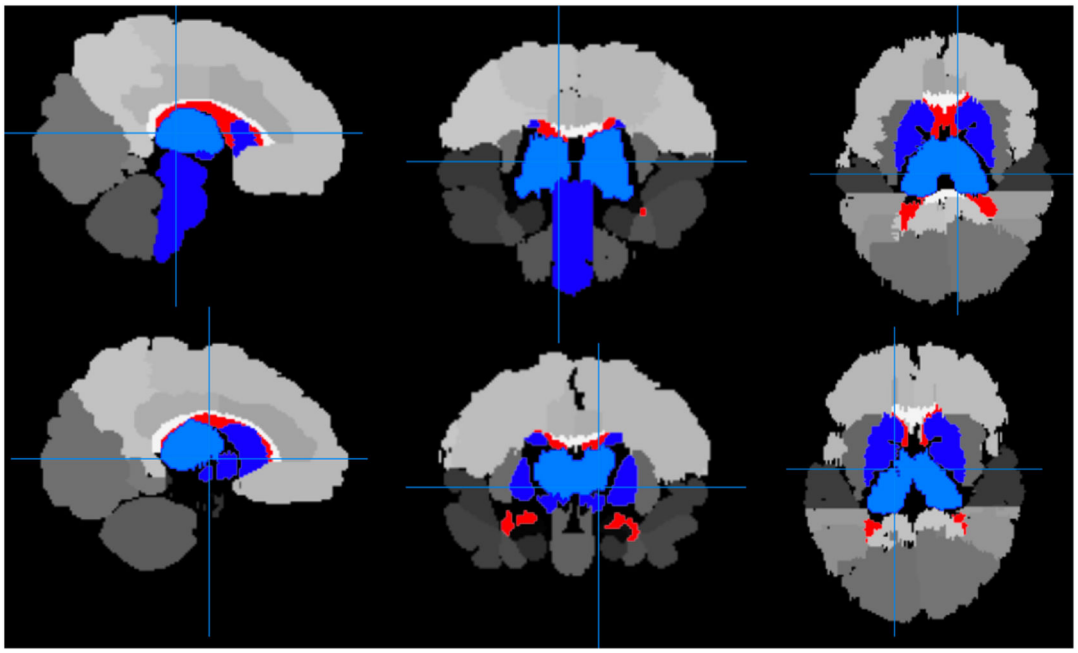

Fig. 2.

Brain templates in sagittal, coronal, and axial orientations (left to right) demonstrating regional brain volumes significantly associated with the early diagnosis of cerebral palsy (CP) when correcting for postmenstrual age only (top row) and all covariates of interest (bottom row). Red volumes are positively associated with early CP (ventricles); blue volumes are negatively associated with early CP; light blue = thalamus (top and bottom); dark blue = deep nuclear gray matter (top and bottom) and brainstem (top); gray/white volumes are not significant.

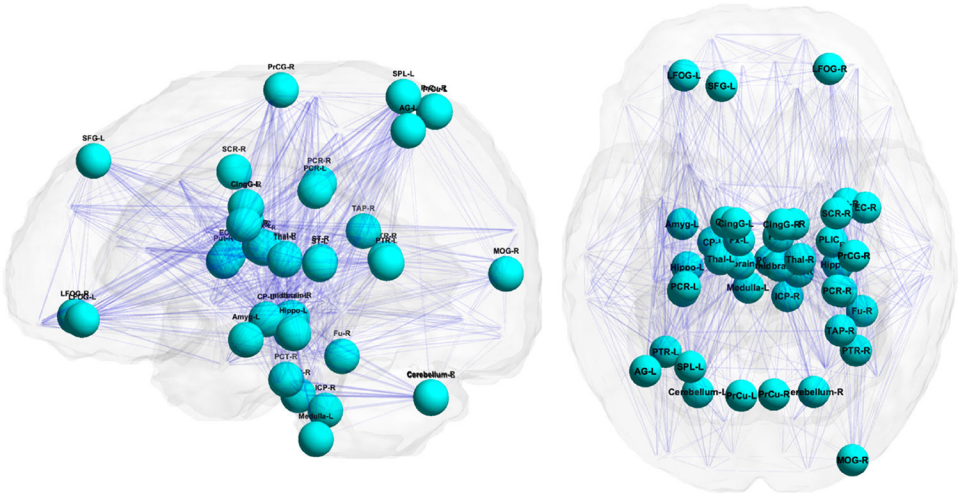

Fig. 3.

Nodes in which local efficiency was negatively associated with early CP diagnosis correcting for PMA, GA, sex, BPD, ROP, and maternal magnesium therapy and adjusting for FDR.

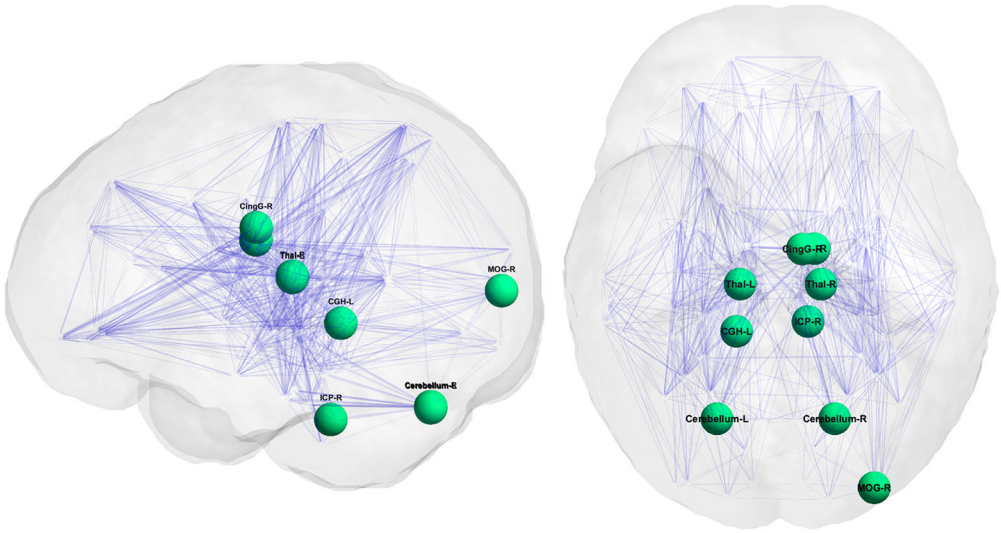

Fig. 4.

Nodes in which clustering coefficient was negatively associated with early CP diagnosis correcting for PMA, GA, sex, BPD, ROP, and maternal magnesium therapy and adjusting for FDR.

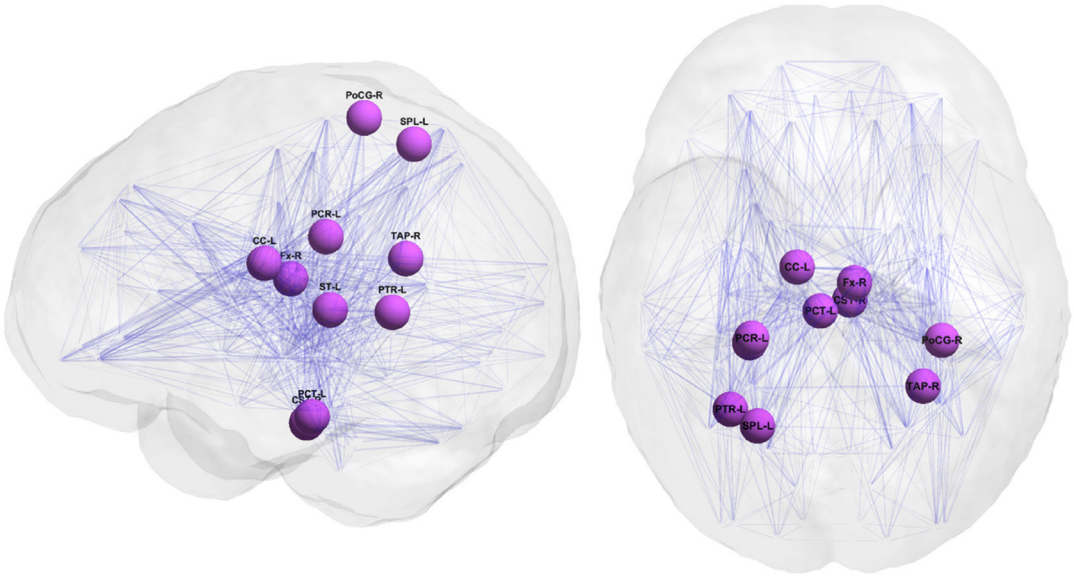

Fig. 5.

Nodes in which strength was negatively associated with early CP diagnosis, correcting for PMA, GA, sex, BPD, ROP, and maternal magnesium therapy and adjusting for FDR.

Table 1

Baseline characteristics of the final very preterm cohort and the excluded infants.

Characteristics	Final Cohort (*n* = 364)	Excluded (*n* = 31)	*p*-value
Antenatal steroids (completed course), *n* (%)	335 (92.03)	27 (87.09)	0.31
Gestational age, weeks, mean (SD)	29.31 (2.44)	28.69 (2.82)	0.14
Birth weight, grams, mean (SD)	1302.17 (448.03)	1201.84 (441.99)	0.09
Male, *n* (%)	190 (52.20)	20 (64.52)	0.20
Severe retinopathy of prematurity, *n* (%)	17 (4.67)	2 (6.45)	0.65
Bronchopulmonary dysplasia, *n* (%)	124 (34.07)	17 (54.84)	0.03
Late onset sepsis, *n* (%)	34 (9.34)	6 (19.35)	0.11
Postnatal steroids (dexamethasone), *n* (%)	55 (15.11)	5 (16.13)	0.80
Maternal magnesium therapy	310 (86.16)	22 (70.97)	0.07
Maternal education (college degree or higher), *n* (%) *	152 (45.10)	10 (35.71)	0.43
Household income above $60,000, *n* (%) **	152 (46.48)	9 (33.33)	0.23
Moderate to severe injury on structural MRI, *n* (%)	37 (10.16)	11 (35.48)	0.0004

* 27 included infants and 3 excluded infants did not have maternal education data.

** 27 included infants and 4 excluded infants did not have income data.

Table 2

Regional graph theory metrics significantly related to early CP diagnosis.

Region	Local Efficiency Odds ratio [95% CI] *p-value*	Clustering Coefficient Odds ratio [95% CI] *p-value*	Strength Odds ratio [95% CI] *p-value*
Corpus callosum-L (CC-L)	2.44 [1.49, 3.85] 2.86×10^{-4}		2.22 [1.33, 3.70] 2.12×10^{-3}
Corpus callosum-R (CC-R)	2.63 [1.64, 4.35] 5.51×10^{-5}	2.00 [1.25, 3.13] 3.74×10^{-3}	
Posterior limb of the internal capsule-R (PLIC-R)	2.04 [1.27, 3.23] 3.25×10^{-3}		
Superior corona radiata -R (SCR-R)	1.96 [1.23, 3.03] 4.11×10^{-3}		
Posterior corona radiata- L (PCR-L)	2.08 [1.35, 3.23] 9.26×10^{-4}		2.04 [1.28, 3.23] 2.66×10^{-3}
Posterior corona radiata-R (PCR-R)	2.04 [1.30, 3.23] 2.10×10^{-3}		
Cingulum hippocampal part-L (CGH-L)		2.04 [1.23, 3.33] 5.56×10^{-3}	
Fornix-L (FX-L)	2.08 [1.37, 3.2] 5.46×10^{-4}		
Fornix-R (Fx-R)	2.70 [1.64, 4.54] 7.13×10^{-5}		2.22 [1.43, 3.45] 4.44×10^{-4}
Stria terminalis-L (ST-L)	1.92 [1.25, 3.03] 3.37×10^{-3}		1.92 [1.25, 2.94] 2.77×10^{-3}
Stria terminalis-R (ST-R)	2.27 [1.45, 3.57] 4.56×10^{-4}		
Tapetum-R (Tap-R)	1.96 [1.27, 3.03] 2.64×10^{-3}		1.96 [1.27 3.13] 2.63×10^{-3}
External capsule-R (EC-R)	1.92 [1.20, 3.03] 5.92×10^{-3}		
Posterior thalamic radiation-L (PTR-L)	2.33 [1.45, 3.70] 4.52×10^{-4}		1.85 [1.22, 2.86] 4.24×10^{-3}
Posterior thalamic radiation-R (PTR-R)	1.85 [1.19, 2.94] 6.95×10^{-3}		
Thalamus-L (Thal-L)	3.22 [1.96, 5.26] 5.68×10^{-6}	2.94 [1.72, 5.00] 7.26×10^{-5}	

Region	Local Efficiency Odds ratio [95% CI] *p-value*	Clustering Coefficient Odds ratio [95% CI] *p-value*	Strength Odds ratio [95% CI] *p-value*
Thalamus-R (Thal-R)	2.63 [1.61, 4.35] 9.26×10^{-5}	2.04 [1.27, 3.23] 2.99×10^{-3}	
Putamen-R (Put-R)	2.17 [1.33, 3.45] 1.67×10^{-3}		
Cerebral peduncle-L (CP-L)	2.17 [1.38, 3.33] 6.57×10^{-4}		
Corticospinal tract-R (CST-R)			2.22 [1.41, 3.45] 5.42×10^{-4}
Middle cerebellar peduncle-R (MCP-R)	1.75 [1.18, 2.63] 6.35×10^{-3}		
Inferior cerebellar peduncle-R (ICP-R)	2.08 [1.41, 3.13] 2.10×10^{-4}	2.12 [1.35, 3.33] 9.33×10^{-4}	
Pontine crossing tract-L (PCT-L)			2.17 [1.32, 3.57] 2.19×10^{-3}
Pontine crossing tract-R (PCT-R)	1.82 [1.18, 2.78] 6.76×10^{-3}		
Midbrain-L (Midbrain-L)	2.08 [1.30, 3.33] 1.98×10^{-3}		
Midbrain-R (Midbrain-R)	1.82 [1.16, 2.78] 7.86×10^{-3}		
Medulla oblongata-L (Medulla-L)	1.64 [1.18, 2.33] 3.61×10^{-3}		
Superior frontal gyrus-L (SFG-L)	1.96 [1.22, 3.03] 5.03×10^{-3}		
Lateral fronto-orbital gyrus-L (LFOG-L)	2.04 [1.27, 3.23] 3.01×10^{-3}		
Lateral fronto-orbital gyrus-R (LFOG-R)	2.22 [1.37, 3.57] 1.38×10^{-3}		
Precentral gyrus-R (PrCG-R)	2.04 [1.27, 3.23] 2.56×10^{-3}		
Postcentral gyrus-R (PoCG-R)			2.08 [1.37, 3.13] 4.68×10^{-4}
Superior parietal lobule-L (SPL-L)	1.82 [1.18, 2.86] 7.04×10^{-3}		2.04 [1.32, 3.13] 1.38×10^{-3}
Precuneus-L (PrCu-L)	1.85 [1.20, 2.86] 5.20×10^{-3}		

Region	Local Efficiency Odds ratio [95% CI] *p-value*	Clustering Coefficient Odds ratio [95% CI] *p-value*	Strength Odds ratio [95% CI] *p-value*
Precuneus-R (PrCu-R)	2.04 [1.39, 3.03] 3.52×10^{-4}		
Cingular gyrus-L CingG-L	1.81 [1.22, 2.70] 3.76×10^{-3}		
Cingular gyrus-R CingG-R	2.33 [1.52, 3.45] 7.83×10^{-5}	1.92 [1.23, 2.94] 4.02×10^{-3}	
Angular gyrus-L (AG-L)	2.22 [1.37, 3.57] 1.07×10^{-3}		
Fusiform gyrus-R (Fu-R)	1.89 [1.19, 3.03] 7.43×10^{-3}		
Middle occipital gyrus-R (MOG-R)	2.78 [1.64, 4.55] 1.18×10^{-4}	2.63 [1.49, 4.55] 6.71×10^{-4}	
Amygdala-L (Amyg-L)	1.72 [1.19, 2.50] 4.22×10^{-3}		
Hippocampus-L (Hippo-L)	1.85 [1.22, 2.78] 3.66×10^{-3}		
Hippocampus-R (Hippo-R)	2.13 [1.35, 3.33] 1.08×10^{-3}		
Cerebellum-R (Cerebellum-R)	2.27 [1.47, 3.45] 1.47×10^{-3}	2.50 [1.52, 4.17] 2.98×10^{-3}	
Cerebellum-L (Cerebellum-L)	1.92 [1.28, 2.94] 1.87×10^{-4}	1.96 [1.27, 3.13] 3.01×10^{-4}	

*All analyses were corrected for PMA at MRI scan, GA, sex, BPD, ROP, and maternal magnesium therapy and adjusted for FDR.